

# RSC Advances



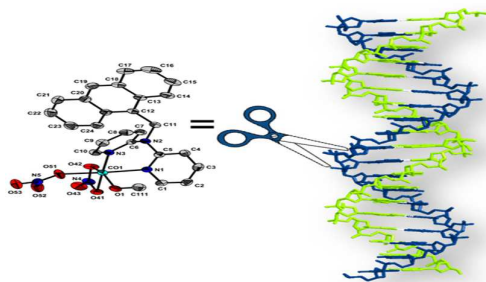
This is an *Accepted Manuscript*, which has been through the Royal Society of Chemistry peer review process and has been accepted for publication.

*Accepted Manuscripts* are published online shortly after acceptance, before technical editing, formatting and proof reading. Using this free service, authors can make their results available to the community, in citable form, before we publish the edited article. This *Accepted Manuscript* will be replaced by the edited, formatted and paginated article as soon as this is available.

You can find more information about *Accepted Manuscripts* in the [Information for Authors](#).

Please note that technical editing may introduce minor changes to the text and/or graphics, which may alter content. The journal's standard [Terms & Conditions](#) and the [Ethical guidelines](#) still apply. In no event shall the Royal Society of Chemistry be held responsible for any errors or omissions in this *Accepted Manuscript* or any consequences arising from the use of any information it contains.

## Graphical Abstract



Divalent metal complexes of dipyriddyamine ligand with an anthracene moiety induced considerable oxidative DNA cleavage in the presence hydrogen peroxide and dioxygen.

## Synthesis, DNA binding profile and DNA cleavage pathway of divalent metal complexes

Nataraj Chitrapriya,<sup>a</sup> Jong Heon Shin,<sup>a</sup> In Hong Hwang,<sup>b</sup> Youngmee Kim,<sup>c</sup> Cheal Kim,<sup>b\*</sup>

Seog K. Kim<sup>a\*</sup>

<sup>a</sup> Department of Chemistry, Yeungnam University, 280 Daehak-Ro, Gyeongsan, Gyeongbuk 712-749, Republic of Korea. Fax: +82-53-815-5412; Tel: +82-53-810-2362; E-mail: [seogkim@yu.ac.kr](mailto:seogkim@yu.ac.kr)

<sup>b</sup> Department of Fine Chemistry and Department of Interdisciplinary Bio IT Materials, Seoul National University of Science and Technology, Seoul 139-743, Republic of Korea. Fax: +82-2-973-9149; Tel: +82-2-970-6693; E-mail: [chealkim@seoultech.ac.kr](mailto:chealkim@seoultech.ac.kr)

<sup>c</sup> Department of Chemistry and Nano Science, Ewha Womans University, Seoul 120-750, Republic of Korea

**Keywords:** Divalent metal complexes, DNA cleavage, Linear dichroism, Artificial nucleases, Reactive oxygen species

## Abstract

Complexes of dipyriddyamine based ligand with an anthracene moiety containing divalent metal ions Co(II), Cu(II), Ni(II), Zn(II) and Cd(II) were characterized structurally. The experimental results showed that they can induce considerable oxidative DNA cleavage in the presence hydrogen peroxide and dioxygen. The Zn(II) complex did not show any appreciable cleavage activity, whereas the Cd(II) and Ni(II) complexes were moderately active. On the other hand, Cu(II) and Co(II) complex showed the formation of a significant quantity of linear DNA resulting from the double-strand breaks. Mechanistic studies revealed the involvement of HO• and the superoxide anion to be the reactive species in the scission process in aerobic media. A mechanism involving either the Fenton or the Haber–Weiss reaction was proposed for the DNA cleavage mediated by these complexes. The Cu(II) complex could also cleave the double stranded calf thymus DNA (ds DNA) in the presence of activators, most likely *via* an oxidative mechanism, whereas the activity of the other complexes was negligible under similar reaction conditions. The kinetic aspects of ds DNA cleavage with the Cu(II) are detailed. The interaction of the five metal complexes with ds DNA was investigated by UV absorption and linear dichroism studies, and the mode of complexes binding to ds DNA is proposed.

## INTRODUCTION

Iron bleomycin (BLM) was the first reported natural product to cleave DNA in an oxidative pathway through the generation of radical species that abstract a hydrogen from the sugar moiety,<sup>1-3</sup> and its importance was soon recognized because of its novel and broad spectrum antitumor properties.<sup>4-8</sup> The therapeutic efficacy of BLM was proposed to be related to its ability to promote the oxidative degradation of DNA and RNA and damage other molecules in the cell.<sup>9-14</sup> The less frequent double strand cleavage (1 for every 6-20 single strand cleavages) is believed to be responsible for the cytotoxic effects of BLM. Double-strand DNA (dsDNA) cleavage is the result of two successive strand scissions in opposite strands in close proximity to each other, resulting in a double-strand break.<sup>15</sup> Ds DNA cleavage is important in terms of its greater cell lethality than that from single-strand cleavage.<sup>16</sup> Similarly, in vitro DNA damage using “chemical nucleases” is a topic of major interest for elucidating the genetic mechanisms of the natural enzymes involved in DNA repair, signal transduction and drug development.<sup>17-20</sup> Artificial nucleases must be efficient and unique in order to mimic the biological function of the enzymes and compete with the innate cellular DNA repair machinery. Among the strategies available for the design of artificial nucleases, the use of transition metal complexes to produce different types of DNA cleavage in the presence of O<sub>2</sub> with or without sequence specificity has attracted interest.<sup>21-24</sup>

Generally, DNA cleavage reactions proceed by targeting various constituents of DNA, such as the nucleic bases, deoxyribose sugar moiety and phosphodiester linkage. Oxidative processes generally form toxic reactive oxygen species involving a photo or redox active metal center that causes damage to the sugar moiety via the direct abstraction of the deoxyribose H1' hydrogen atom and/or nucleobase resulting in the formation of fragmented

species.<sup>21,25-29</sup> The chemistry of nucleic acid degradation by synthetic nucleases has been the subject of numerous studies.<sup>18,30-36</sup> On the other hand, only a limited number of reports have examined the actual rates of product formation (kinetics) during chemical nuclease induced DNA scissoring.<sup>37-40</sup> A recent development in the field of DNA cleavage are measurements of the reaction kinetics of the drug-mediated DNA cleavage by the linear dichroism (LD) technique.<sup>41-44</sup> Here, we report the synthesis and characterization of various transition metal complexes containing a dipyridylamine-based ligand bearing the anthracene moiety (Fig. 1). Anthracene moiety is one of fused aromatic hydrocarbons and is expected to intercalate between DNA base pair, thereby, enhance the binding efficiency to DNA. The ability of the complexes to promote the cleavage of two different DNA, namely, pBR322 plasmid DNA, and calf thymus DNA, was investigated. In the latter case, the detailed degradation kinetics were evaluated using the LD technique. The binding mode of the metal complexes to calf thymus DNA was also examined by absorption and LD spectroscopy.

## EXPERIMENTAL SECTION

### Materials and Instrumentation

All chemicals were used as received unless stated otherwise. Calf thymus DNA (referred to as dsDNA) was purchased from Sigma and dissolved in a 5 mM cacodylate buffer (pH 7.0) containing 1 mM EDTA and 100 mM NaCl by gentle shaking at 4 °C. The dsDNA solution was dialyzed several times against 5 mM cacodylate buffer (pH 7.0) at 4 °C. The dsDNA concentration was measured using the extinction coefficient:  $\varepsilon_{260\text{nm}} = 6700 \text{ M}^{-1}\text{cm}^{-1}$ . The pBR 322 plasmid DNA (referred to as sc DNA) stock solution (1mg/mL) was purchased from New England Biolabs (Massachusetts, USA).

The UV/Vis spectra were recorded on a Cary 100 spectrometer. The LD spectrum and time-dependent LD magnitude at 260 nm were measured either on a J-715 or J-810 spectropolarimeter (Jasco, Tokyo, Japan) equipped with an inner rotating flow cell. The result were analyzed using the OriginPro 8.0 program (OriginLab Co., Northampton, MA, USA). The  $^1\text{H}$  and  $^{13}\text{C}$  nuclear magnetic resonance (NMR) spectra were recorded on a Varian 400 MHz spectrometer and chemical shifts were recorded in ppm. The electrospray ionization mass spectra (ESI-MS) were collected on a Thermo Finnigan (San Jose, CA, USA) LCQ<sub>TM</sub> Advantage MAX quadrupole ion trap instrument by infusing the samples directly into the source using a manual method. The spray voltage was set to 4.2 kV, and the capillary temperature was at 80 °C. Elemental analysis for carbon, nitrogen, and hydrogen was carried out using a Flash EA 1112 elemental analyzer (thermo) at the Organic Chemistry Research Center of Sogang University, Korea.

### LD Measurement

LD is defined as the difference in the absorbance of an oriented sample between the light polarized parallel and perpendicular. LD is a powerful technique for determining the binding mode of a drug to DNA by providing the angle,  $\alpha$ , between the electric transition moment of the DNA-bound drug and the local DNA helix axis using the following equation.

$$LD' = \frac{LD}{A_{iso}} = 1.5S(3\cos^2\alpha - 1) \quad (1)$$

where  $LD'$ , denotes the reduced LD, which is defined by division of the measured LD by the isotropic absorption spectrum,  $A_{iso}$ . The orientation factor,  $S$ , can be calculated by assuming an angle of  $86^\circ$  between the DNA base plane and the local DNA helix axis. Once  $S$  is calculated, the angle,  $\alpha$ , can be obtained easily. As the magnitude of LD in the DNA absorption wavelength region depends on the length and flexibility of DNA, the time-dependent changes in the LD magnitude can be used to probe DNA cleavage in real-time.<sup>43,44</sup>

### Agarose gel electrophoresis

In the gel electrophoresis experiments, supercoiled pBR322 DNA was treated with metal complexes dissolved in 5mM cacodylate buffer, and the mixture was incubated at  $37^\circ\text{C}$ . At the end of incubation, the reaction was quenched by adding loading buffer (7 mM EDTA, 0.15% bromophenol blue, 0.15% xylene cyanol and 75% glycerol). The samples were then

analyzed by 1% agarose gel electrophoresis for 7 h at 25 V, 400 mA. The gel was stained in tris-acetate-EDTA (TAE) buffer containing 0.5 mg mL<sup>-1</sup> ethidium bromide, 20 mM tris acetate and 1 mM EDTA. The extent of sc DNA cleavage was visualized by UV trans-illumination and photographed using an Olympus C-5060 camera. To test for the presence of reactive oxygen species (ROS) generated during strand scission, a range of reactive oxygen intermediate scavengers were added to the reaction mixtures and the samples were treated as described above. The data is reported as the average of the cleavage experiments performed at least in triplicate.

#### Synthesis of N-((anthracen-9-yl)methyl)-N-(pyridin-2-yl)pyridin-2-amine (ADPA)

2,2-Dipyridyl amine (0.1747 g, 1mmol) and KOH (0.1120 g, 2 mmol) were dissolved in 10 mL of dimethylformamide. Subsequently, 9-(chloromethyl)anthracene (0.2267g, 1 mmol) was added, and the reaction mixture was stirred for 1 day at room temperature. The solution was extracted 3 times with methylene water and chloride. The organic phase was separated and the solvent was removed in vacuo. The pure product was obtained by column chromatography (silica gel, methylene chloride/ ethyl acetate 10:1) in 63.9 % yield. IR (KBr):  $\nu(\text{cm}^{-1}) = 1583(\text{m}), 1469(\text{s}), 1422(\text{s}), 1345(\text{w}), 1300(\text{m}), 1153(\text{w}), 979(\text{m}), 891(\text{m}), 776(\text{s}), 726(\text{s})$ . <sup>1</sup>H NMR (DMSO-*d*<sub>6</sub>, 400MHz)  $\delta$  8.53 (d, 2H, 9.6 Hz), 8.46 (s, 1H), 8.33(d, 2H, 4.8 Hz), 8.0 (d, 2H, 9.6 Hz), 7.48 (m, 6H), 6.90 (d-d, 2H, 7.2, 5.2 Hz), 6.45 (d, 2H, 8.4 Hz), 6.31 (s,2H) ppm. <sup>13</sup>C NMR (DMSO-*d*<sub>6</sub>, 100MHz)  $\delta$  158, 148, 138, 131, 131, 129, 129, 127, 126, 125, 118, 116, 43 ppm. HRMS (ESI): *m/z* calcd for C<sub>25</sub>H<sub>19</sub>N<sub>3</sub>+H<sup>+</sup>([M+H<sup>+</sup>]), 362.17; found,

362.20. Anal. calcd for  $C_{25}H_{19}N_3$ (361.44): C, 78.52; H, 6.22; N, 15.26. Found: C, 78.57; H, 6.20 ; N, 15.14 %.

#### Synthesis of $[Co(ADPA)(NO_3)_2(CH_3OH)]$ (1)

ADPA (9.0 mg, 0.025 mmol) was dissolved in 0.5 mL methylene chloride and 0.5 mL of a methanol solution of  $Co(NO_3)_2 \cdot 6H_2O$  (7.4 mg, 0.025 mmol) was added to the solution. After one day, 7 mL of pentane was layered carefully above the complex solution. Crystals suitable for X-ray analysis were obtained in two days. The yield was 7.3 mg (51.0%). IR (KBr):  $\nu(\text{cm}^{-1}) = 3251(\text{brw}), 2973(\text{w}), 1600(\text{m}), 1433(\text{s}), 1300(\text{s}), 1234(\text{m}), 1160(\text{m}), 1016(\text{s}), 898(\text{m}), 729(\text{s})$ . Anal. Calc. for  $C_{26}H_{23}CoN_5O_7$  (576.42), **1**: C, 54.18; H, 4.02; N, 12.15. Found: C, 54.45; H, 3.83; N, 12.41%.

#### Synthesis of $[Cu(ADPA)(NO_3)_2(CH_3OH)]$ (2)

ADPA (18.01 mg, 0.05 mmol) and  $Cu(NO_3)_2 \cdot 2.5H_2O$  (5.9 mg, 0.025 mmol) were dissolved in 1 mL methanol. After one day, 7 mL of isopropyl ether was layered carefully above the complex solution. Crystals suitable for X-ray analysis were obtained in two days. The yield was 8.1 mg (56.1%). IR (KBr):  $\nu(\text{cm}^{-1}) = 3390(\text{br}), 2973(\text{w}), 1602(\text{w}), 1462(\text{s}), 1279(\text{s}), 1163(\text{m}), 1071(\text{w}), 1016(\text{m}), 899(\text{m}), 730(\text{s})$ . Anal. Calc. for  $C_{26}H_{23}CuN_5O_7$  (581.04), **2**: C, 53.75; H, 3.99; N, 12.05. Found: C, 53.21; H, 4.32; N, 12.23%.

**Synthesis of [Ni(ADPA)(NO<sub>3</sub>)<sub>2</sub>(CH<sub>3</sub>OH)] (3)**

ADPA (18.01 mg, 0.05 mmol) and Ni(NO<sub>3</sub>)<sub>2</sub>·6H<sub>2</sub>O (7.3 mg, 0.025 mmol) were dissolved in 1 mL methanol. After one day, 7 mL of diethyl ether was layered carefully above the complex solution. Crystals suitable for X-ray analysis were obtained in a week. The yield was 6.5 mg (45.2%). IR (KBr):  $\nu(\text{cm}^{-1}) = 3320(\text{brw}), 2974(\text{w}), 1601(\text{w}), 1434(\text{s}), 1305(\text{s}), 1234(\text{m}), 1160(\text{m}), 1018(\text{m}), 898(\text{m}), 730(\text{s})$ . Anal. Calc. for C<sub>26</sub>H<sub>23</sub>N<sub>5</sub>NiO<sub>7</sub> (576.18), **3**: C, 54.20; H, 4.02; N, 12.15. Found: C, 54.35; H, 3.82; N, 12.34%.

**Synthesis of [Zn(ADPA)(NO<sub>3</sub>)<sub>2</sub>] (4)**

ADPA (9.0 mg, 0.025 mmol) was dissolved in 0.5 mL methylene chloride and 0.5 mL of a methanol solution of Zn(NO<sub>3</sub>)<sub>2</sub>·6H<sub>2</sub>O (7.6 mg, 0.025 mmol) was added to the solution. After one day, 7 mL of pentane was layered carefully above the complex solution. Crystals suitable for X-ray analysis were obtained in two weeks. The yield was 8.3 mg (60.4%). IR (KBr):  $\nu(\text{cm}^{-1}) = 1602(\text{m}), 1488(\text{s}), 1440(\text{s}), 1346(\text{m}), 1296(\text{s}), 1233(\text{m}), 1135(\text{w}), 886(\text{m}), 780(\text{m}), 736(\text{s})$ . Anal. Calc. for C<sub>25</sub>H<sub>19</sub>N<sub>5</sub>O<sub>6</sub>Zn (550.84), **4**: C, 54.51; H, 3.48; N, 12.71. Found: C, 54.72; H, 3.27; N, 12.95%.

**Synthesis of [Cd(ADPA)(NO<sub>3</sub>)<sub>2</sub>(CH<sub>3</sub>OH)] (5)**

ADPA (9.0 mg, 0.025 mmol) was dissolved in 0.5 mL methylene chloride and 0.5 mL of a methanol solution of Cd(NO<sub>3</sub>)<sub>2</sub>·4H<sub>2</sub>O (7.9 mg, 0.025 mmol) was added into the solution.

After one day, 7 mL of pentane was layered carefully above the complex solution. Crystals suitable for X-ray analysis were obtained in one week. The yield was 8.8 mg (56.1%). IR (KBr):  $\nu(\text{cm}^{-1}) = 3409(\text{br}), 2974(\text{w}), 1598(\text{w}), 1432(\text{s}), 1299(\text{s}), 1163(\text{m}), 1032(\text{m}), 953(\text{m}), 794(\text{m}), 730(\text{s})$ . Anal. Calc. for  $\text{C}_{26}\text{H}_{23}\text{CdN}_5\text{O}_7$  (629.9), **5**: C, 49.58; H, 3.68; N, 11.12. Found: C, 49.24; H, 3.88; N, 11.15%.

### **X-ray Crystallography.**

X-ray diffraction (XRD) of **1-5** was performed on a Bruker SMART APEX diffractometer using a monochromatic Mo  $\text{K}\alpha$  ( $\lambda = 0.71073 \text{ \AA}$ ) incident beam. Each crystal was mounted on a glass fiber. The CCD data was integrated and scaled using the Bruker-S SAINT software package, and the structure was solved and refined using SHELXTL V6.12.<sup>45</sup> All hydrogen atoms were placed in the calculated positions. Table 1 lists the crystallographic data for complexes **1 - 5**. Tables 2 and S1-S5 list the selected bond distances and angles. Structural information was deposited at the Cambridge Crystallographic Data Center (CCDC reference numbers are 948383 - 948387 for **1-5**).

## RESULTS AND DISCUSSION

### Structures descriptions

The reactions of  $M(\text{NO}_3)_2$  with ADPA yielded the following structures:  $[\text{M}(\text{ADPA})(\text{NO}_3)_2(\text{CH}_3\text{OH})]$  ( $M = \text{Co}$  (**1**),  $\text{Cu}$  (**2**),  $\text{Ni}$  (**3**), and  $\text{Cd}$  (**5**)). The ligand ADPA, two nitrate anions, and a methanol molecule coordinate to a metal ion to form a distorted octahedral geometry (Fig. 2 for **1**, Fig. S1 for **2**, Fig. S2 for **3**, and Fig. S3 for **5**). The octahedral coordination is constructed by two N atoms of a chelating ADPA ligand, two O atoms of a chelating nitrate ion ( $M\text{-O}_{\text{nitrate}}$  range, one O atom of the other monodentate nitrate ion, and one O atom of a methanol molecule (see Table S1-S3 and S5 for bond distances)). In contrast, an ADPA ligand with  $\text{Zn}(\text{NO}_3)_2$  produces  $[\text{Zn}(\text{ADPA})(\text{NO}_3)_2]$  (**4**). The ligand ADPA and two nitrate anions coordinate to a Zn(II) anion to form a distorted trigonal pyramidal geometry with two N atoms of a chelating ADPA ligand (Zn-N distances of 2.037(3) and 2.038(3) Å), two O atoms of an asymmetric chelating nitrate (bond distances of Zn-O<sub>nitrate</sub> of 2.031(3) and 2.484(4) Å), and one O atom of a monodentate nitrate ion (Zn-O<sub>nitrate</sub> distance of 1.965(3) Å) (Fig. 2 and Table S4).

### Oxidative DNA cleavage mediated by the complexes as a function of time

The cleavage efficiency of metal complexes **1-5** in the presence of activator ( $\text{H}_2\text{O}_2$ ) was probed by agarose gel electrophoresis. The DNA plasmid was incubated with metal complexes (20  $\mu\text{M}$ ) and  $\text{H}_2\text{O}_2$  (500  $\mu\text{M}$ ) for various time intervals (0-6 h) at pH 7.5 and 37 °C. The cleavage efficiency increased with time, and the quantity of plasmid DNA decreased

gradually due to the degradation of sc DNA (form I) to the nicked form (form II) and linear DNA (form III). Lane 1 in Fig. 3(a) shows the control DNA without any added complex. DNA incubated with either the complex or peroxide alone does not show any apparent change in the supercoiled form (Fig. 3(a) lanes 2, 3). In the presence of peroxide, the metal complexes can cleave supercoiled DNA. This suggests that the DNA cleavage mediated by these complexes should adopt an oxidative mechanism. The observed distribution of supercoiled and nicked DNA in the agarose gels provides a measure of the degree of DNA cleavage by these complexes. Complex **1** can also degrade sc DNA to linear form to a certain extent after 6 h incubation time. As shown in Fig. 3(a), lane 6, linear DNA began to appear after 2 h incubation once a significant amount of nicked DNA (>55%) had formed in the reaction without smearing. A single cut or nick on a strand of sc DNA relaxes the supercoiling, which leads to form II. A second cut on the complementary strand, within approximately 12 base pairs from the original cut site, linearizes the DNA to form III. Therefore, **1** must have cut the DNA at least twice to convert it from form I to form III.

Among the five complexes examined, Fig. 3(b) (lanes 1-7) shows that the cleavage is quite efficient, and form I is transformed almost completely to open circular DNA (form II) in the presence of 20  $\mu\text{M}$  of complex **2**. Form III is detectable only after all the supercoiled plasmid has been nicked and finally, the DNA is degraded (to smaller undetectable fragments) as indicated by a smear on the gel (lanes 6 and 7, Fig. 3(b)). Complex **2** shows higher cleavage activity than the other complexes. The smear DNA fragments that appeared in the lanes show that the breakage products can be attributed to the poor selectivity. Interestingly, significant differences were observed in the product distribution between the **1** and **2** complexes. Using complex **2** as catalyst, linear DNA is formed after the complete conversion

of Form I to Form II, which is the result of extensive single strand cleavage activity (Fig. 3(b)). Direct double-strand DNA cleavage was not observed in this case. In contrast, a significant amount of linear DNA is formed, even with 36% of the supercoiled DNA remaining, when complex **1** was used as catalysts. This suggests that other mechanisms in addition to single strand cleavage are responsible for the formation of linear DNA, such as direct double strand cleavage. Complex **2** nicks the plasmid DNA and degrades the linear form much more efficiently than complex **1**, which produces well-defined electrophoresis bands of linear DNA. In addition, the appearance of a well-defined electrophoresis band for linear DNA suggests that the production of linear DNA by complex **1** is due to a non-random strand scission event, because random cutting is expected to produce a smear of fragments in the scission reaction as observed for complex **2**.

In contrast to complexes **1** and **2**, the incubation of supercoiled DNA with **3** and **5** (20  $\mu$ M) up to 6 h did not produce any linear DNA under similar reaction conditions (Fig. 4(a) and (c)). These results show that complexes **3** and **5** exhibit only moderate activity on the single strand breaks: the sc DNA form was not converted fully to the nicked form (49% and 47% of the SC form and 51% and 53% of the nicked form produced, for complexes **3** and **5**, respectively), whereas double strand cleavage (form III) was not observed. The continuous increase in the amount of nicked DNA during 6 h with **3** and **5** showed that these complexes remained active during this time. In the presence of 20  $\mu$ M of **4**, no significant change in the proportion of the supercoiled DNA was observed over a period of 6 h (Fig. 4(b)), suggesting that this complex is not an efficient nuclease.

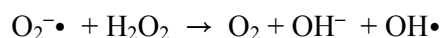
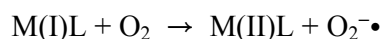
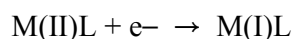
### Investigation of ROS in the DNA cleavage reaction

To examine the cleavage mechanism, the metal complex-mediated DNA cleavage was examined using several different potential radical scavengers to identify the intermediate reactive oxygen species (ROS). The strong inhibition of DNA cleavage mediated by the complexes (**3** and **5**) was observed upon the addition of DMSO (lane 8, Fig. 4(a) and (c)), indicating that the hydroxyl radical is involved in the cleavage process. Catalase also prevents the nucleolytic process, confirming that hydrogen peroxide is also essential in the DNA strand scission (lane 11, Fig. 4(a) and (c)). By adding tiron, the efficiency of the conversion of sc DNA to nicked DNA by complexes **3** and **5** was decreased. The cleavage potency of complexes **3** and **5** was unaffected by the singlet oxygen scavenger, sodium azide. Mechanistic studies with the reactive oxygen species (ROS) scavengers confirmed that hydrogen peroxide, the hydroxyl radical and superoxide anion are essential diffusible intermediates for single strand breakage by complexes **3** and **5**. In the case of complex **1** (Fig. 3, lane 13), the addition of tiron has no inhibition effect on the cleavage of the linear form but it can inhibit the nicked form of the cleavage process. The experimental results (Fig. 3, lane 11-14) showed that the quenching of HO<sup>•</sup>, superoxide anion and H<sub>2</sub>O<sub>2</sub> can inhibit the activity of complex **1** efficiently. As shown in Fig. 3(b), lane 9, no obvious inhibition was observed for the nicked form in the presence of sodium azide, whereas it barely inhibited the linear DNA cleavage, suggesting that singlet oxygen is not involved in the single strand cleavage process through complex **2**. On the other hand, the addition of DMSO and catalase (Fig. 3 (b), lanes 8 and 11) had an obvious inhibitory effect on DNA cleavage. The generation of HO<sup>•</sup>, superoxide anion and H<sub>2</sub>O<sub>2</sub> appears to contribute to the production of DNA frank strand breaks by complex **2**. These free radicals abstract the most accessible and exposed sugar

hydrogen and initiate oxidative cleavage, leading to DNA-cleavage products. The difference in the formation of ROS during cleavage may be indicative of the different DNA cleavage efficiency of the metal complexes.

### **Mechanism of DNA cleavage**

In this study, the mechanism of oxidative DNA damage induced by metal complexes was examined in detail. Transition-metal-mediated hydroxyl radical production occurs via a number of routes; two well-known pathways are the Fenton and the Haber–Weiss mechanism. The Haber–Weiss reaction is the most probable mechanism for the DNA scission induced by the metal complexes **1-5** because gel electrophoresis showed that the hydroxyl radical, superoxide anion and hydrogen peroxide play critical roles in DNA scission. The Haber-Weiss reaction involves the reaction of superoxide with H<sub>2</sub>O<sub>2</sub> to produce dioxygen, hydroxide and OH•. The possible mechanism of DNA damage induced by divalent transition metal complexes are as follows:



### **Cleavage of dsDNA probed by LD**

The magnitude of the LD spectrum of dsDNA depends on a range of factors including the flexibility and length of DNA. More flexible and shorter DNA results in less orientation, and consequently decreases the LD magnitude.<sup>43,44</sup> Fig. 5(A) shows the change in the LD spectrum of DNA in the presence of complex **2** and H<sub>2</sub>O<sub>2</sub>. The LD at the time of mixing appeared to be negative with a similar shape to the absorption spectrum as expected from the set-up adopted in this study.<sup>46,47</sup> The magnitude of LD decreased gradually with time without changing its shape, suggesting increased flexibility and/or shortened DNA length. When the LD magnitude was plotted as a function of time, the decrease can be explained by a single exponential decay curve, suggesting that the cleavage followed first-order kinetics. This is in contrast to a previous report.<sup>44</sup> The decrease in LD magnitude due to oxidative dsDNA cleavage, induced by Fe(EDTA)<sup>2+</sup>, H<sub>2</sub>O<sub>2</sub> and ascorbate, was attributed to two sequential first order reactions. The fast reaction was assigned to the cleavage of one of the double strands and the slow reaction represented a cut of the complementary strand near the first cleavage.<sup>44</sup> The former reaction results in increased flexibility of DNA, whereas the latter causes shortening of the DNA strand. The observed first order reaction (Fig. 5(A)) may be understood by the similar rates for these two sequential reaction. In contrast to the fast cleavage of one of the strands in the presence of the Fenton reagents,<sup>44</sup> this reaction is so slow for complex **2**, which is indistinguishable from the second step. The rate constant calculated from the fitted single exponential curve was  $0.32 \pm 0.02 \text{ h}^{-1}$ . Other complexes including complex **1**, which showed intermediate activity in the scDNA cleavage probed by electrophoresis, did not result in a significant decrease in LD magnitude, even after 5 hours incubation, suggesting that these complexes are not as active in the oxidative cleavage of dsDNA as complex **2**. Although this discrepancy is not completely understood, it might be related to the difference in binding mode and/or binding affinity between scDNA and dsDNA.

The reduction of the central metal is an important step in producing reactive oxygen species, as shown in the previous section. Complex **2** contains Cu(II). Similar studies using metal complexes possessing a range of central metal ions (Cu(II), Cd(II), Ni(II), and Zn(II)) with ligands, such as (2,2'-dipyridylamine)<sub>2</sub>(NO<sub>3</sub>)<sub>x</sub>, also showed significantly high oxidative dsDNA cleavage activity for Cu(II).<sup>42,48</sup> Therefore, we assume that the redox potential, i.e., the ability of electron donation of the metal complexes, might be the main reason for the different efficiency in the oxidative cleavage of dsDNA.

Similar study using structurally related [Cu(dipicolylamine)(NO<sub>3</sub>)<sub>2</sub>] complex, which lacks anthracene moiety compared to the complex **2**, exhibited no cleavage activity.<sup>49</sup> It cleaved neither scDNA nor dsDNA as it was shown by electrophoresis and linear dichroism technique, respectively. Therefore, it is clear that anthracene moiety take an important role in the DNA cleavage activity of the complex **2**. Although the role of anthracene moiety is unclear at this stage, there are two conceivable possibilities. The first possibility is that hydrophobicity of anthracene moiety may help the complex **2** to be closer to interior of DNA resulting in a tighter binding, although it is not intercalated between DNA base pairs (see following section). The second one is that the presence of anthracene may cause change in the electron density at the central Cu metal, thereby possibly helps reduction of Cu (II) to Cu(I).

### **Binding mode of the complexes to dsDNA**

All metal complexes produced a strong absorption band at 255 nm, which coincides with the DNA absorption region, and the anthracene absorption band between 340 nm and 400 nm.

Upon the association with DNA, all metal complexes showed absorbance in the anthracene absorption region. In addition, the shape of the LD spectrum for the DNA-metal complex adducts was similar regardless of the nature of the central metal ion. Therefore, the binding mode of the metal complexes, which is a possible factor, resulting in different activity, is unlikely to be essential. Here, the binding mode of only a representative complex, complex **2**, to DNA will be discussed to avoid repetition. The intensity of the absorption spectrum in the anthracene absorption region of complex **2** (and other complexes) decreased with increasing dsDNA concentration, whereas the shape of the absorption spectrum remained unchanged (Fig 6(A)). Normally, a red-shift and hypochromism (or hyperchromism) in the absorption spectrum of the drug are produced when bound to DNA. For the intercalators, a large red-shift and hypochromism are often observed as a result of stacking between the aromatic moiety of the intercalator and the DNA bases, in addition to the change in the environmental polarity. In the case of the minor groove binding drug, such as 4',6-diamidino-2-phenylindole or Hoechst 33258, such a change originates from a change in the conformation of the unfused aromatic drugs. The observed decrease in absorbance without a shift in the peak location for complex **2** when associated with dsDNA was different from the intercalator or minor groove binding drugs. Nevertheless, a change in the absorption spectrum allows the Benesi-Hildebrand plot to be constructed according to equation (2).

$$\frac{1}{\Delta A_{371nm}} = -\frac{1}{(\epsilon_b - \epsilon_f)[L_t]} + \frac{1}{(\epsilon_b - \epsilon_f)[L_t]K_{BH}[dsDNA]} \quad (2)$$

In this equation,  $\epsilon$  denotes the molar extinction coefficient, and  $b$  and  $f$  represent the bound and free metal complex, respectively.  $[L_t]$  and  $\Delta A_{371nm}$  are the total complex concentration and change in absorbance at 371 nm, respectively. The association constant for the dsDNA-

complex **2** adduct formation,  $K_{BH} = 4.91(\pm 0.20) \times 10^4 \text{ M}^{-1}$ , was calculated from the ratio of the slope to the intercept. The association for the other complexes were in a similar range.

Fig 6(B) shows the  $LD^f$  spectrum of the dsDNA-complex **2** adduct. In the DNA absorption region, the magnitude of  $LD^f$  tended to decrease, suggesting that the binding of complex **2** resulted in a bent or kink at or near the binding site. The positive contribution observed near 290 nm for the dsDNA-complex **2** adduct might have originated from the positive contribution of the dsDNA bound complex because the anthracene moiety possesses an absorption band in this region. On the other hand, the  $LD^f$  signal in this region was mixed with that of the DNA bases, preventing a detailed analysis of the binding geometry of anthracene moiety of the complex **2**. The small negative band with vibrational structures was observed in the 340 ~ 420 nm region. If a planar compound is intercalated between the DNA base pairs, its planar moiety is almost parallel to the DNA bases and perpendicular to the local DNA helix axis. A large negative  $LD^f$  signal in the absorption region of the intercalator with a magnitude similar to or larger than the DNA absorption region is expected in this case. This type of  $LD^f$  spectrum has been reported for classical intercalators, such as ethidium or 9-aminoacridine.<sup>46,47</sup> On the other hand, if any compound binds along the minor groove, as observed for classical minor groove binding molecules, such as 4',6-diamidino-2-phenylindole and Hoechst 33258, the long axis of the compound lies at an angle of almost 45° with respect to the local DNA helix axis, resulting in a positive  $LD^f$  in the absorption region of the minor groove binding compounds. The observed small negative  $LD^f$  signal in the complex **2** absorption region (340 ~ 420 nm) of the dsDNA-complex **2** adduct (and adducts formed with other complexes) does not coincide with these two classical cases. The orientation factor ( $S$  in equation (1)) can be calculated from the  $LD^f$  value at 260 nm by

assuming a mean angle of  $86^\circ$  between the DNA bases and the local DNA helix axis. Once the  $S$  value is known, it is straightforward to calculate the angle,  $\alpha$ , which is the angle between the in-plane electric transition moment of the anthracene moiety and the local DNA helix axis. The calculated angle was  $56^\circ \sim 58^\circ$ , suggesting that the molecular plane of the anthracene moiety tilts at this angle, which matches neither the classical intercalator nor the minor groove binding compounds. Rejecting the possibility of these two typical binding modes, complex **2** may be located at the major groove or at the surface of dsDNA. At the surface of dsDNA, the positively charged metal complexes may interact with negatively charged phosphate groups through an electrostatic interaction.

## CONCLUSION

Co(II), Cu(II), Ni(II), Zn(II), and Cd(II) complexes with an anthracene-attached dipyridylamine-based ligand were synthesized, and their structures were determined. From the X-ray structures, only the Zn(II) complex showed a four coordinated structure; the others exhibited a hexa-coordinated structure including a methanol molecule and two nitrates. The Cu(II) complex efficiently cleaved both dsDNA and sc DNA. The Co(II) complex exhibited intermediate activity in oxidative sc DNA cleavage. The other complexes were almost inactive in DNA cleavage. All the complexes appear to bind at the surface of ds DNA via an electrostatic interaction with the phosphate groups of ds DNA.

## Acknowledgement

This study was supported by Korea Research Foundation (NRF-2015R1A2A2A09001301 and NRF-2014R1A2A1A11051794).

## References

1. S.M. Hecht and R.M. Burger, *Chem. Rev.*, 1998, **98**, 1153-1169.
2. W.K. Pogozelski and T.D. Tullius, *Chem. Rev.*, 1998, **98**, 1089-1107.
3. J. Chen and J. Stubbe, *Nat. Rev. Cancer*, 2005, **5**, 102-112.
4. S.M. Hecht, *J. Nat. Prod.*, 2000, **63**, 158-168.
5. J. Chen, J. Stubbe, *Curr. Opin. Chem. Biol.*, 2004, **8**, 175-181.
6. A. Decker, M.S. Chow, J.N. Kemsley, N. Lehnert and E.I. Solomon, *J. Am. Chem. Soc.* 2006, **128**, 4719-4733.
7. S.E. Hashimoto, B.X. Wang and S.M. Hecht, *J. Am. Chem. Soc.*, 2001, **123**, 7437-7438.
8. D.H. Petering, W.B. Li, C.W. Xia, C.Q. Zhao and W.E. Antholine, *J. Inorg. Biochem.*, 2001, **86**, 85-85.
9. B.J. Carter, E. de Vroom, E.C. Long, G.A. Van der Marel, J.H. van Boom and S.M. Hecht, *Proc. Natl. Acad. Sci. U.S.A.*, 1990, **87**, 9373-9377.
10. C.E. Holmes and S.M. Hecht, *J. Biol. Chem.*, 1993, **268**, 25909-25913.
11. S.M. Hecht, *Bioconjugate Chem.*, 1994, **5**, 513-526.
12. J. Stubbe, F. J.W. Kozarich, W. Wu and D.E. Vanderwall, *Acc. Chem. Res.*, 1996, **29**, 322-330.
13. R.M. Burger, *Chem Rev.*, 1998, **98**, 1153-1169.
14. S. M. Hecht, *J. Nat. Prod.*, 2000, **63**, 158-168.
15. D. Freifelder and B. Trumbo, *Biopolymers*, 1969, **7**, 681-693.
16. L.F. Povirk, *Mutat. Res.*, 1991, **257**, 127-143.
17. A. Sreedhara and J.A. Cowan, *J. Biol. Inorg. Chem.*, 2001, **6**, 337-347.
18. J.A. Cowan, *Curr. Opin. Chem. Biol.*, 2001, **5**, 634-642.

19. C. Liu, M. Wang, T. Zhang and H. Sun, *Coord. Chem. Rev.*, 2004, **248**, 147-168.
20. F. Mancin, P. Scrimin, P. Tecilla and U. Tonellato, *Chem. Commun.*, 2005, **20**, 2540-2548.
21. D.S. Sigman, A. Mazumder and D.M. Perrin, *Chem. Rev.*, 1993, **93**, 2295-2316.
22. G. Pratviel, J. Bernadou and B. Meunier, *Angew. Chem. Int. Ed.*, 1995, **34**, 746-769.
23. F.V. Pamatong, C.A. Detmer and J.R. Bocarsly, *J. Am. Chem. Soc.*, 1996, **118**, 5339-5345.
24. C.-C. Cheng, W.-C. Huang-Fu, K.-C. Hung, P.-J.Chen, W.J. Wang and Y.-J. Chen, *Nucleic Acids Res.*, 2003, **31**, 2227-2233.
25. D.S. Sigman, *Acc. Chem. Res.*, 1986, **19**, 180-186.
26. D.S. Sigman, T.W. Bruice, A. Mazumder and C.L. Sutton, *Acc. Chem. Res.*, 1993, **26**, 98-104.
27. Q. Jiang, N. Xiao, P.F. Shi, Y.G. Zhu and Z.J. Guo, *Coord. Chem. Rev.*, 2007, **251**, 1951-1972.
28. D.-D. Li, J.-L. Tian, W. Gu, X. Liu, H.-H. Zeng and S.-P. Yan, *J. Inorg. Biochem.*, 2011, **105**, 894-901.
29. A.K. Patra, T. Bhowmick, S. Roy, S. Ramakumar and A.R. Chakravarty, *Inorg. Chem.*, 2009, **48**, 2932-2943.
30. T.D. Tullius and J.A. Greenbaum, *Curr. Opin. Chem. Biol.*, 2005, **9**, 127-134.
31. C. Marzano, M. Pellei, F. Tisato and C. Santini, *Anti-Cancer Agents Med. Chem.*, 2009, **9**, 185-211.
32. A. Roigk, R. Hettich and H.J. Schneider, *J. Inorg. Chem.*, 1998, **37**, 751-756.
33. R. Hettich and H.J. Schneider, *J. Am. Chem. Soc.*, 1997, **119**, 5638-5647.
34. A.K. Yatsimirsky, *Coord. Chem. Rev.*, 2005, **249**, 1997-2011.

35. J.R. Morrow, *Curr. Opin. Chem. Biol.*, 2004, **8**, 192-200.
36. M.P. Fitzsimons and J.K. Barton, *J. Am. Chem. Soc.*, 1997, **119**, 3379-3380.
37. D.-D. Li, J.-L. Tian, W. Gu, X. Liu and S.-P. Yan, *J. Inorg. Biochem.*, 2010, **104**, 171-179.
38. S. Anbu, S. Shanmugarajub and M. Kandaswamy, *RSC Adv.*, 2012, **2**, 5349-5357.
39. S. Dhar, P.A.N. Reddy and A.R. Chakravarty, *Dalton Trans.*, 2004, 697-698
40. L. Wei, Y. Shao, M. Zhou, H.-W. Hua and G.-Y. Lu, *Org. Biomol. Chem.*, 2012, **10**, 8484-8492
41. J. Rammo, R. Hettich, A. Rodger and H.J. Schneider, *Chem. Commun.*, 1996, 105-107.
42. K.J. Jang, G.-Y. Yeo, T.S. Cho, G.H. Eom, C. Kim and S.K. Kim, *Biophys. Chem.*, 2010, **148**, 138-143.
43. W. Wang, G.J. Lee, K.J. Jang, T.S. Cho and S.K. Kim, *Nucleic Acids Res.*, 2008, **36**, 1-7. doi:10.1093/nar/gkn370.
44. H.J. Kim, G. Sung, G. Kim, J. Park, B. Jin and S.K. Kim, *Chem. Asian J.*, 2014, **9**, 1341-1348.
45. Bruker, SHELXTL/PC, Version 6.12 for Windows XP, Bruker AXS Inc., Madison, Wisconsin, USA, 2001.
46. A. Rodger and B. Nordén, *Circular Dichroism and Linear Dichroism*. Oxford University Press, Oxford 1997.
47. B. Nordén, M. Kubista and T. Kurucsev, *Q. Rev. Biophys.*, 1992, **25**, 51-170.
48. H.-J. Park, J.H. Kwon, T.-S., Cho, J.M. Kim, I.H. Hwang, C. Kim, S. Kim, J. Kim and S.K. Kim, *J. Inorg. Biochem.*, 2013, **127**, 46-52.
49. J.H. Kwon, H.-J. Park, N. Chitrapriya, T.-S. Cho, S. Kim, J. Kim, I.H. Hwang, C. Kim, and S.K. Kim, *J. Inorg. Biochem.*, 2014, **131**, 79-86.



**Table 1.** Crystallographic Data for Compounds **1 - 5**.

	<b>1</b>	<b>2</b>	<b>3</b>	<b>4</b>	<b>5</b>
Empirical formula	C <sub>26</sub> H <sub>23</sub> CoN <sub>5</sub> O <sub>7</sub>	C <sub>26</sub> H <sub>23</sub> CuN <sub>5</sub> O <sub>7</sub>	C <sub>26</sub> H <sub>23</sub> NiN <sub>5</sub> O <sub>7</sub>	C <sub>25</sub> H <sub>19</sub> ZnN <sub>5</sub> O <sub>6</sub>	C <sub>26</sub> H <sub>23</sub> CdN <sub>5</sub> O <sub>7</sub>
Formula weight	576.42	581.03	576.20	550.82	629.89
Temperature (K)	293(2)	170(2)	170(2)	293(2)	293(2)
Wavelength (Å)	0.71073	0.71073	0.71073	0.71073	0.71073
Space group	P2 <sub>1</sub> /c	P2 <sub>1</sub> /c	P2 <sub>1</sub> /c	P2 <sub>1</sub> 2 <sub>1</sub>	P2 <sub>1</sub> /c
a (Å)	15.259(3)	15.446(3)	15.186(3)	9.5790(19)	15.420(3)
b (Å)	10.425(2)	10.012(2)	10.313(2)	14.734(3)	10.430(2)
c (Å)	16.754(3)	16.856(3)	16.548(3)	16.363(3)	16.718(3)
α (°)	90.00	90.00	90.00	90.00	90.00
β (°)	108.93(3)	109.14(3)	109.05(3)	90.00	107.95(3)
γ (°)	90.00	90.00	90.00	90.00	90.00
Volume(Å <sup>3</sup> )	2521.0(9)	2462.6(9)	2449.7(8)	2309.4(8)	2557.9(9)
Z	4	4	4	4	4
Density (calc.) (Mg/m <sup>3</sup> )	1.519	1.567	1.562	1.584	1.636
Absorption coeff. (mm <sup>-1</sup> )	0.738	0.945	0.851	1.118	0.910
Crystal size (mm <sup>3</sup> )	0.25 x 0.12 x 0.10	0.10 x 0.08 x 0.07	0.25 x 0.10 x 0.10	0.18 x 0.16 x 0.02	0.35 x 0.30 x 0.20
Reflections collected	13736	13151	13378	12937	13970
Independent reflections	4915 [R(int) = 0.0456]	4781 [R(int) = 0.0907]	4811 [R(int) = 0.0364]	4534 [R(int) = 0.0480]	5018 [R(int) = 0.0201]
Data / restraints / parameters	4915 / 0 / 356	4781 / 1 / 356	4811 / 1 / 356	4534 / 0 / 334	5018 / 1 / 356
Goodness-of-fit on F <sup>2</sup>	1.053	1.005	0.996	0.979	1.038
Final R indices [I > 2σ(I)]	R <sub>1</sub> = 0.0469, wR <sub>2</sub> = 0.1081	R <sub>1</sub> = 0.0581, wR <sub>2</sub> = 0.1143	R <sub>1</sub> = 0.0357, wR <sub>2</sub> = 0.0870	R <sub>1</sub> = 0.0416, wR <sub>2</sub> = 0.0868	R <sub>1</sub> = 0.0283, wR <sub>2</sub> = 0.0741
R indices (all data)	R <sub>1</sub> = 0.0780, wR <sub>2</sub> = 0.1193	R <sub>1</sub> = 0.1282, wR <sub>2</sub> = 0.1376	R <sub>1</sub> = 0.0496, wR <sub>2</sub> = 0.0910	R <sub>1</sub> = 0.0660, wR <sub>2</sub> = 0.0959	R <sub>1</sub> = 0.0358, wR <sub>2</sub> = 0.0770
Largest diff. peak and hole (e.Å <sup>-3</sup> )	0.343 and -0.309	0.413 and -0.624	0.335 and -0.269	0.294 and -0.194	0.362 and -0.376

**Table 2.** Selected Bond Distances for **1 - 5**.

	<b>1</b>	<b>2</b>	<b>3</b>	<b>4</b>	<b>5</b>
M-N	2.076(2), 2.119(2)	1.963(4), 1.989(4)	2.0229(17), 2.0543(18)	2.037(3), 2.038(3)	2.2749(18), 2.318(2)
M-O <sub>nitrate</sub>	2.060(2)-2.185(2)	1.984(3), 1.999(3)	2.0659(17)- 2.1462(16)	1.965(3)-2.038(3), 2.484(4)	2.3576(19)- 2.506(2)
M-O <sub>CH<sub>2</sub>OH</sub>	2.072(2)	2.306(3)	2.0543(18)	-	2.3199(19)

## Figure Legends

**Figure 1.** Chemical structures of metal complexes. (A) M = Co(II), Cu(II), Ni(II) and Cd(II), designated by complex **1**, **2**, **3**, and **5**, respectively. (B) M = Zn(II), designated by complex **4**.

**Figure 2.** Crystal structures of complexes **1** and **4** with 30% ellipsoid. All hydrogen atoms were omitted for clarity.

**Figure 3.** (a) Time dependent oxidative DNA cleavage of plasmid pBR322 (50  $\mu\text{M}$ ) in the presence 500  $\mu\text{M}$  of  $\text{H}_2\text{O}_2$  by 20  $\mu\text{M}$  of complex **1** at 37  $^\circ\text{C}$  after incubated for 0-6 h. Lane 1, DNA control; lane 2, DNA+  $\text{H}_2\text{O}_2$ ; lane 3, DNA+**1**; lane 4-10, DNA+**1**+  $\text{H}_2\text{O}_2$  (0-6 h with 1 h increment); lane 11, DNA+**1**+DMSO+  $\text{H}_2\text{O}_2$ ; lane 12, DNA+**1**+ $\text{NaN}_3$ +  $\text{H}_2\text{O}_2$ ; lane 13, DNA+**1**+tiron+  $\text{H}_2\text{O}_2$ ; lane 14, DNA+**1**+catalase+  $\text{H}_2\text{O}_2$  (6 h incubation time).

(b) Time dependent oxidative DNA cleavage of plasmid pBR322 (50  $\mu\text{M}$ ) in the presence 500  $\mu\text{M}$  of  $\text{H}_2\text{O}_2$  by 20  $\mu\text{M}$  of complex **2** at 37  $^\circ\text{C}$  after incubated for 0-60 min. Lane 1-7, DNA+**2**+  $\text{H}_2\text{O}_2$  (0-60 min with 10 min increment); lane 8, DNA+**2**+ DMSO + $\text{H}_2\text{O}_2$ ; lane 9, DNA+**2**+  $\text{NaN}_3$  + $\text{H}_2\text{O}_2$ ; lane 10, DNA+**2**+ tiron + $\text{H}_2\text{O}_2$ ; lane 11, DNA+**2**+ catalase + $\text{H}_2\text{O}_2$  (60 min incubation time)

**Figure 4.** Time dependent oxidative DNA cleavage of plasmid pBR322 (50  $\mu\text{M}$ ) in the presence of 500  $\mu\text{M}$  of  $\text{H}_2\text{O}_2$  by 20  $\mu\text{M}$  of complex **3-5** at 37  $^\circ\text{C}$  after incubated for 0-6 h. (a)

Complex **3**: lane 1-7, DNA+complex+ H<sub>2</sub>O<sub>2</sub> (0-6 h, respectively); lane 8, DNA+complex+DMSO+H<sub>2</sub>O<sub>2</sub>; lane 9, DNA+complex+NaN<sub>3</sub>+H<sub>2</sub>O<sub>2</sub>; lane 10, DNA+complex+tiron+H<sub>2</sub>O<sub>2</sub>; lane 11, DNA+complex+catalase+H<sub>2</sub>O<sub>2</sub> (6 h incubation time). (b) Complex **4**. (c) Complex **5**.

**Figure 5.** (A) Decrease in LD magnitude in the DNA absorption region in the presence of the complex **2** and H<sub>2</sub>O<sub>2</sub>. LD spectra were recorded 0, 1, 2, 3, 4 and 5 h after mixing to the arrow direction. Insertion: Decrease in LD magnitude at 260 nm with respect to the time. Solid red curve in the insertion represents the best fitting single exponential curve. The best fit single-exponential decay curve is shown in the inserted figure. (B) LD spectrum of DNA 5 h after mixing with various metal complexes. [Metal complex] = 20 μM, [DNA] = 500 μM in base and [H<sub>2</sub>O<sub>2</sub>] = 50 μM.

**Figure 6.** (A) Absorption spectrum of the complex **2** in the presence and absence of dsDNA. Only selective concentration of DNA i.e., [dsDNA] = 0, 10, 20, 30, 60 and 90 μM to arrow direction. [Complex **2**] = 15 μM. The reciprocal change in absorbance at 371 nm with respect to reciprocal dsDNA concentration according to equation (2) is inserted. (B) LD<sup>f</sup> spectrum of dsDNA (blue dashed curve) and that of dsDNA-complex **2** adduct (red solid curve). [Complex **2**] = 20 μM and [dsDNA] = 500 μM. H<sub>2</sub>O<sub>2</sub> is absent for both absorption and LD<sup>f</sup> spectra.

Figure 1

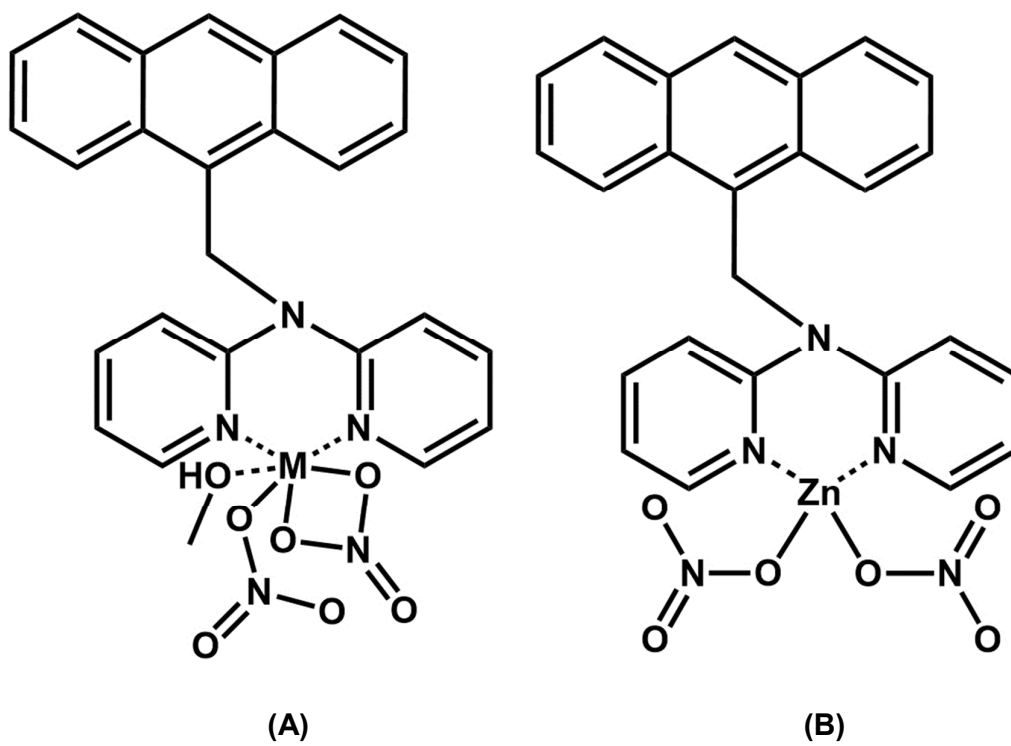


Figure 2

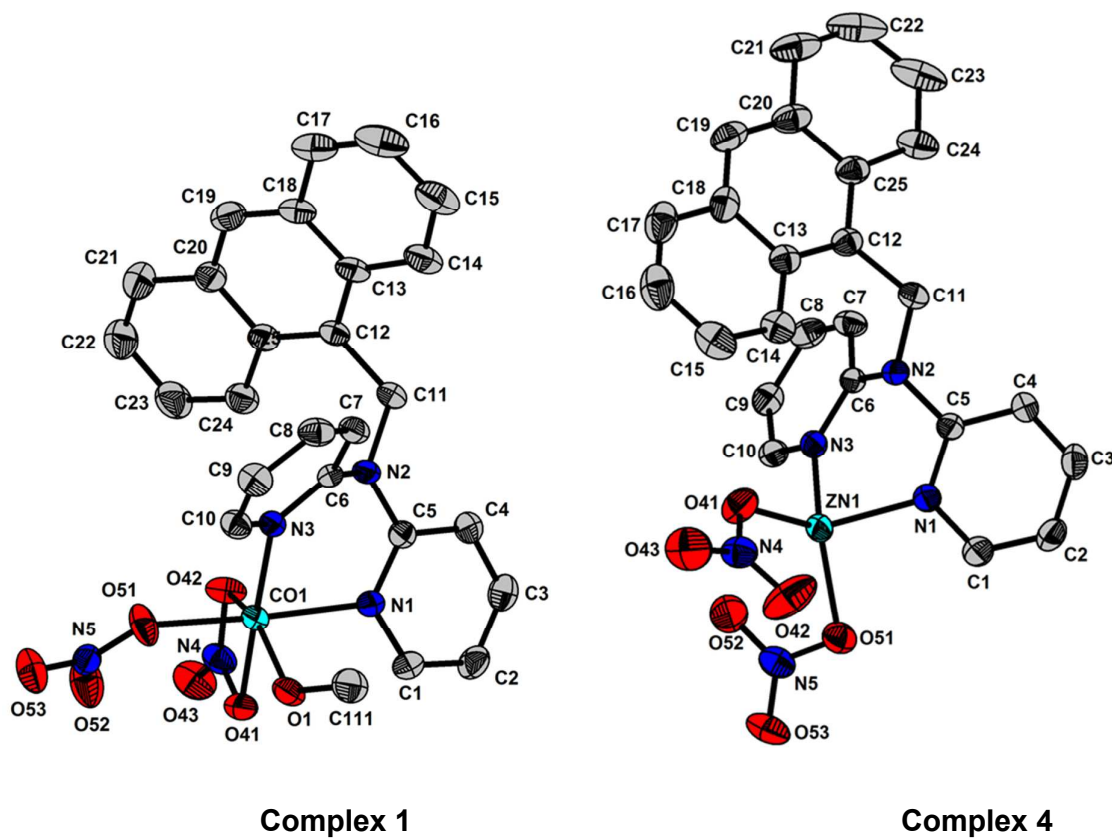


Figure 3

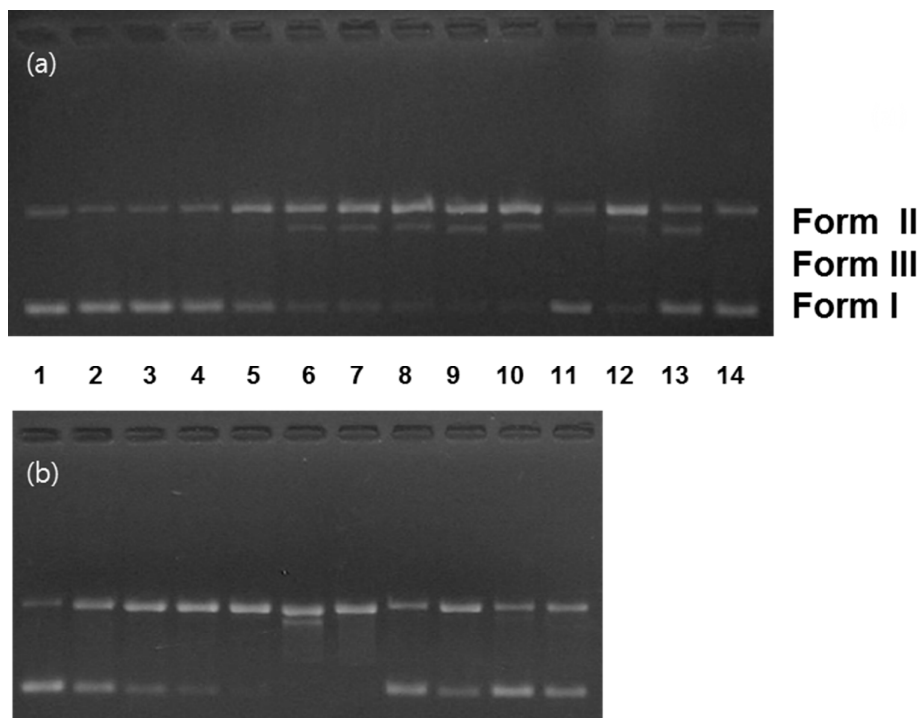


Figure 4

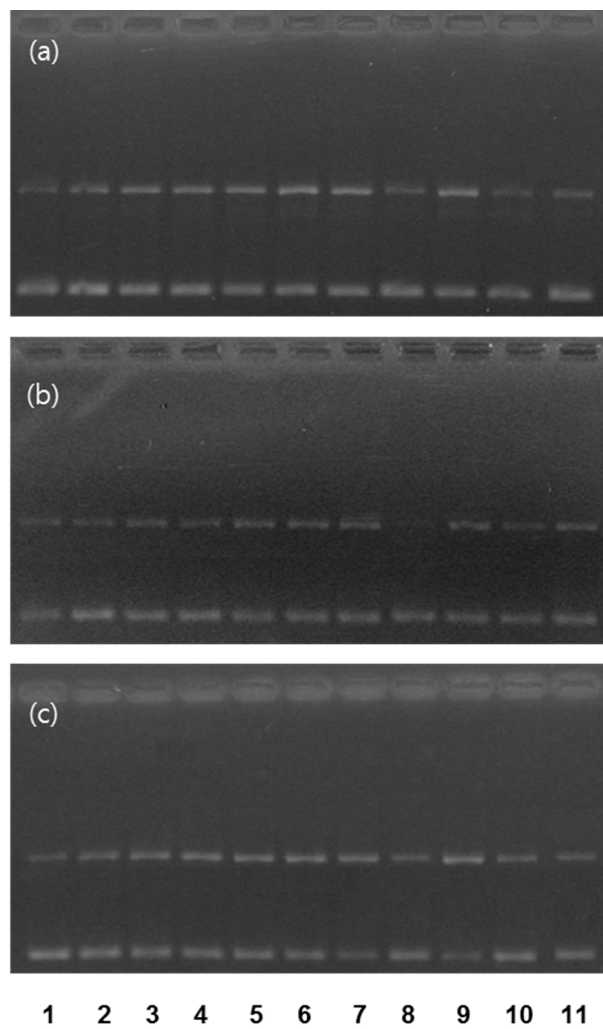


Figure 5

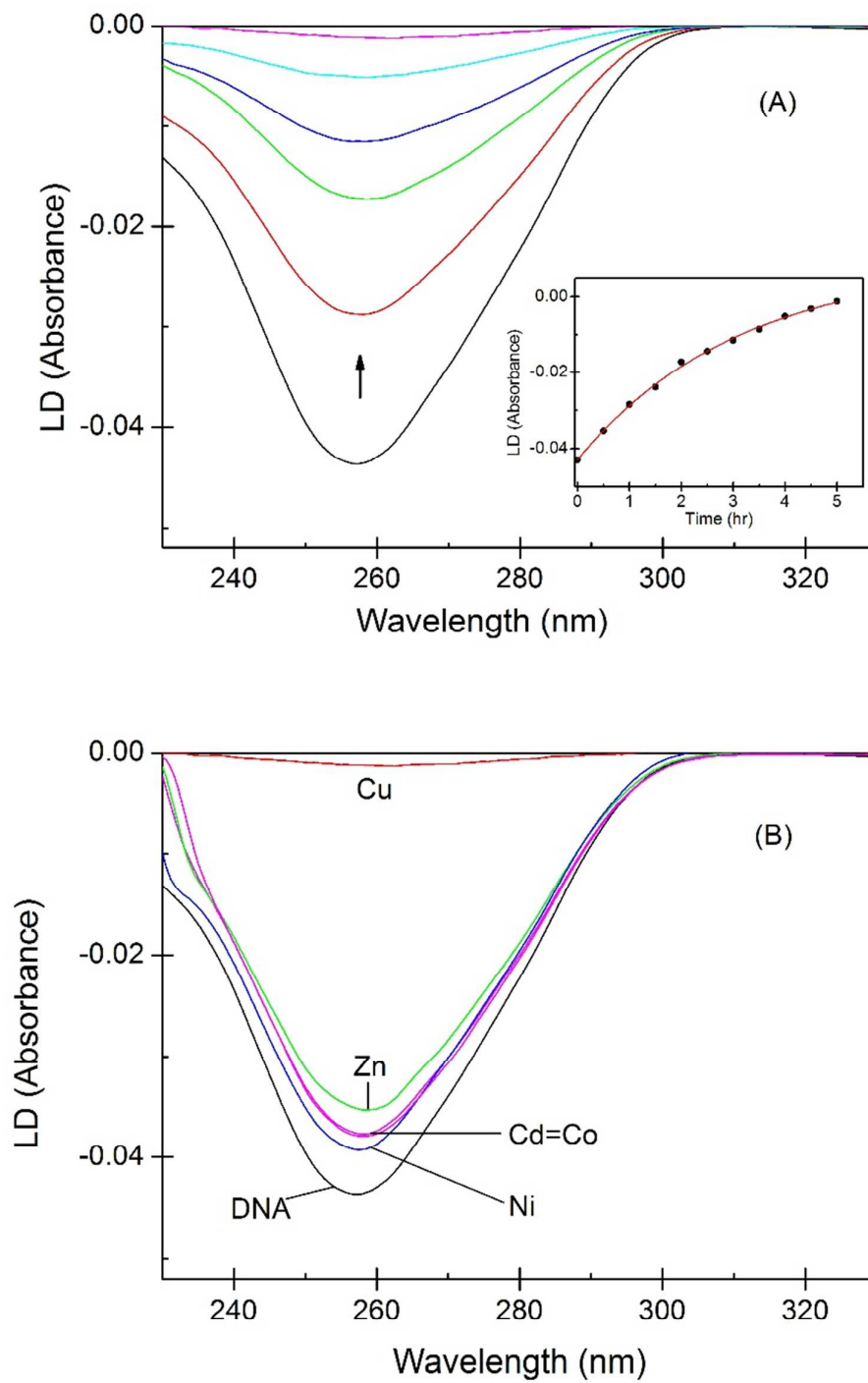


Figure 6

